Y production in U + U collisions at sqrt[s_{NN}]=193 GeV measured with the STAR experiment

L. Adamczyk *et al.* (STAR Collaboration)

Υ production in U+U collisions at $\sqrt{s_{NN}} = 193$ GeV with the STAR experiment

L. Adamczyk,[1] J. K. Adkins,[2] G. Agakishiev,[3] M. M. Aggarwal,[4] Z. Ahammed,[5] I. Alekseev,[6,7] D. M. Anderson,[8] R. Aoyama,[9] A. Aparin,[3] D. Arkhipkin,[9] E. C. Aschenauer,[9] M. U. Ashraf,[10] A. Attri,[4] G. S. Averichev,[3] X. Bai,[11] V. Bairathi,[12] R. Bellwied,[13] A. Bhasin,[14] A. K. Bhati,[4] P. Bhattarai,[15] J. Bielcik,[16] J. Bielcikova,[17] L. C. Bland,[9] I. G. Bordyuzhin,[6] J. Bouchet,[18] J. D. Brandenburg,[19] A. V. Brandin,[7] I. Bunzarov,[3] J. Butterworth,[19] H. Caines,[20] M. Calderón de la Barca Sánchez,[21] J. M. Campbell,[22] D. Cebra,[21] I. Chakaberia,[9] P. Chaloupka,[16] Z. Chang,[8] A. Chatterjee,[5] S. Chattopadhyay,[5] J. H. Chen,[23] X. Chen,[24] J. Cheng,[10] M. Cherney,[25] W. Christie,[9] G. Contin,[26] H. J. Crawford,[27] S. Das,[28] L. C. De Silva,[25] R. R. Debbe,[9] T. G. Dedovich,[3] J. Deng,[29] A. A. Derevschikov,[30] L. Didenko,[9] C. Dilks,[31] X. Dong,[26] J. L. Drachenberg,[32] J. E. Draper,[21] C. M. Du,[24] L. E. Dunkelberger,[33] J. C. Dunlop,[9] L. G. Efimov,[3] J. Engelage,[27] G. Eppley,[19] R. Esha,[33] S. Esumi,[9] O. Evdokimov,[34] O. Eyser,[9] R. Fatemi,[2] S. Fazio,[9] P. Federic,[17] J. Fedorisin,[3] Z. Feng,[11] P. Filip,[3] E. Finch,[35] Y. Fisyak,[9] C. E. Flores,[21] L. Fulek,[1] C. A. Gagliardi,[8] D. Garand,[36] F. Geurts,[19] A. Gibson,[37] M. Girard,[38] L. Greiner,[26] D. Grosnick,[37] D. S. Gunarathne,[39] Y. Guo,[40] A. Gupta,[14] S. Gupta,[14] W. Guryn,[9] A. I. Hamad,[18] A. Hamed,[8] R. Haque,[12] J. W. Harris,[20] L. He,[36] S. Heppelmann,[21] S. Heppelmann,[31] A. Hirsch,[36] G. W. Hoffmann,[15] S. Horvat,[20] H. Z. Huang,[33] B. Huang,[34] T. Huang,[41] X. Huang,[10] P. Huck,[11] T. J. Humanic,[22] G. Igo,[33] W. W. Jacobs,[42] A. Jentsch,[15] J. Jia,[9,43] K. Jiang,[40] S. Jowzaee,[44] E. G. Judd,[27] S. Kabana,[18] D. Kalinkin,[42] K. Kang,[10] K. Kauder,[44] H. W. Ke,[9] D. Keane,[18] A. Kechechyan,[3] Z. Khan,[34] D. P. Kikoła,[38] I. Kisel,[45] A. Kisiel,[38] L. Kochenda,[7] D. D. Koetke,[37] L. K. Kosarzewski,[38] A. F. Kraishan,[39] P. Kravtsov,[7] K. Krueger,[46] L. Kumar,[4] M. A. C. Lamont,[9] J. M. Landgraf,[9] K. D. Landry,[33] J. Lauret,[9] A. Lebedev,[9] R. Lednicky,[3] J. H. Lee,[9] Y. Li,[10] C. Li,[40] X. Li,[39] W. Li,[23] X. Li,[40] T. Lin,[42] M. A. Lisa,[22] F. Liu,[11] Y. Liu,[8] T. Ljubicic,[9] W. J. Llope,[44] M. Lomnitz,[18] R. S. Longacre,[9] X. Luo,[11] S. Luo,[34] G. L. Ma,[23] R. Ma,[9] L. Ma,[23] Y. G. Ma,[23] N. Magdy,[43] R. Majka,[20] A. Manion,[26] S. Margetis,[18] C. Markert,[15] H. S. Matis,[26] D. McDonald,[13] S. McKinzie,[26] K. Meehan,[21] J. C. Mei,[29] Z. W. Miller,[34] N. G. Minaev,[30] S. Mioduszewski,[8] D. Mishra,[12] B. Mohanty,[12] M. M. Mondal,[8] D. A. Morozov,[30] M. K. Mustafa,[26] B. K. Nandi,[47] Md. Nasim,[33] T. K. Nayak,[5] G. Nigmatkulov,[7] T. Niida,[44] L. V. Nogach,[30] T. Nonaka,[9] J. Novak,[48] S. B. Nurushev,[30] G. Odyniec,[26] A. Ogawa,[9] K. Oh,[49] V. A. Okorokov,[7] D. Olvitt Jr.,[39] B. S. Page,[9] R. Pak,[9] Y. X. Pan,[33] Y. Pandit,[34] Y. Panebratsev,[3] B. Pawlik,[50] H. Pei,[11] C. Perkins,[27] P. Pile,[9] J. Pluta,[38] K. Poniatowska,[38] J. Porter,[26] M. Posik,[39] A. M. Poskanzer,[26] N. K. Pruthi,[4] M. Przybycien,[1] J. Putschke,[44] H. Qiu,[36] A. Quintero,[39] S. Ramachandran,[2] R. L. Ray,[15] R. Reed,[51,51] M. J. Rehbein,[25] H. G. Ritter,[26] J. B. Roberts,[19] O. V. Rogachevskiy,[3] J. L. Romero,[21] J. D. Roth,[25] L. Ruan,[9] J. Rusnak,[17] O. Rusnakova,[16] N. R. Sahoo,[8] P. K. Sahu,[28] I. Sakrejda,[26] S. Salur,[26] J. Sandweiss,[20] A. Sarkar,[47] J. Schambach,[15] R. P. Scharenberg,[36] A. M. Schmah,[26] W. B. Schmidke,[9] N. Schmitz,[52] J. Seger,[25] P. Seyboth,[52] N. Shah,[23] E. Shahaliev,[3] P. V. Shanmuganathan,[18] M. Shao,[40] M. K. Sharma,[14] A. Sharma,[14] B. Sharma,[4] W. Q. Shen,[23] Z. Shi,[26] S. S. Shi,[11] Q. Y. Shou,[23] E. P. Sichtermann,[26] R. Sikora,[1] M. Simko,[17] S. Singha,[18] M. J. Skoby,[42] D. Smirnov,[9] N. Smirnov,[20] W. Solyst,[42] L. Song,[13] P. Sorensen,[9] H. M. Spinka,[46] B. Srivastava,[36] T. D. S. Stanislaus,[37] M. Stepanov,[36] R. Stock,[45] M. Strikhanov,[7] B. Stringfellow,[36] T. Sugiura,[9] M. Sumbera,[17] B. Summa,[31] Y. Sun,[40] Z. Sun,[24] X. M. Sun,[11] B. Surrow,[39] D. N. Svirida,[6] Z. Tang,[40] A. H. Tang,[9] T. Tarnowsky,[48] A. Tawfik,[53] J. Thäder,[26] J. H. Thomas,[26] A. R. Timmins,[13] D. Tlusty,[19] D. Todoroki,[9] M. Tokarev,[3] S. Trentalange,[33] R. E. Tribble,[8] P. Tribedy,[9] S. K. Tripathy,[28] O. D. Tsai,[33] T. Ullrich,[9] D. G. Underwood,[46] I. Upsal,[22] G. Van Buren,[9] G. van Nieuwenhuizen,[9] R. Varma,[47] A. N. Vasiliev,[30] R. Vertesi,[17] F. Videbæk,[9] S. Vokal,[3] S. A. Voloshin,[44] A. Vossen,[42] G. Wang,[33] J. S. Wang,[24] F. Wang,[36] Y. Wang,[10] Y. Wang,[11] J. C. Webb,[9] G. Webb,[9] L. Wen,[33] G. D. Westfall,[48] H. Wieman,[26] S. W. Wissink,[42] R. Witt,[54] Y. Wu,[18] Z. G. Xiao,[10] G. Xie,[40] W. Xie,[36] K. Xin,[19] Z. Xu,[9] H. Xu,[24] N. Xu,[26] J. Xu,[11] Y. F. Xu,[23] Q. H. Xu,[29] Y. Yang,[24] Y. Yang,[41] S. Yang,[40] Q. Yang,[40] Y. Yang,[11] C. Yang,[40] Z. Ye,[34] Z. Ye,[34] L. Yi,[20] K. Yip,[9] I. -K. Yoo,[49] N. Yu,[11] H. Zbroszczyk,[38] W. Zha,[40] J. Zhang,[29] Z. Zhang,[23] J. Zhang,[24] S. Zhang,[23] X. P. Zhang,[10] J. B. Zhang,[11] Y. Zhang,[40] S. Zhang,[40] J. Zhao,[36] C. Zhong,[23] L. Zhou,[40] X. Zhu,[10] Y. Zoulkarneeva,[3] and M. Zyzak[45]

(STAR Collaboration)

[1]*AGH University of Science and Technology, FPACS, Cracow 30-059, Poland*
[2]*University of Kentucky, Lexington, Kentucky, 40506-0055*
[3]*Joint Institute for Nuclear Research, Dubna, 141 980, Russia*
[4]*Panjab University, Chandigarh 160014, India*
[5]*Variable Energy Cyclotron Centre, Kolkata 700064, India*
[6]*Alikhanov Institute for Theoretical and Experimental Physics, Moscow 117218, Russia*
[7]*National Research Nuclear University MEPhI, Moscow 115409, Russia*
[8]*Texas A&M University, College Station, Texas 77843*
[9]*Brookhaven National Laboratory, Upton, New York 11973*
[10]*Tsinghua University, Beijing 100084*
[11]*Central China Normal University, Wuhan, Hubei 430079*
[12]*National Institute of Science Education and Research, Bhubaneswar 751005, India*

^{13}*University of Houston, Houston, Texas 77204*
^{14}*University of Jammu, Jammu 180001, India*
^{15}*University of Texas, Austin, Texas 78712*
^{16}*Czech Technical University in Prague, FNSPE, Prague, 115 19, Czech Republic*
^{17}*Nuclear Physics Institute AS CR, 250 68 Prague, Czech Republic*
^{18}*Kent State University, Kent, Ohio 44242*
^{19}*Rice University, Houston, Texas 77251*
^{20}*Yale University, New Haven, Connecticut 06520*
^{21}*University of California, Davis, California 95616*
^{22}*Ohio State University, Columbus, Ohio 43210*
^{23}*Shanghai Institute of Applied Physics, Chinese Academy of Sciences, Shanghai 201800*
^{24}*Institute of Modern Physics, Chinese Academy of Sciences, Lanzhou, Gansu 730000*
^{25}*Creighton University, Omaha, Nebraska 68178*
^{26}*Lawrence Berkeley National Laboratory, Berkeley, California 94720*
^{27}*University of California, Berkeley, California 94720*
^{28}*Institute of Physics, Bhubaneswar 751005, India*
^{29}*Shandong University, Jinan, Shandong 250100*
^{30}*Institute of High Energy Physics, Protvino 142281, Russia*
^{31}*Pennsylvania State University, University Park, Pennsylvania 16802*
^{32}*Lamar University, Physics Department, Beaumont, Texas 77710*
^{33}*University of California, Los Angeles, California 90095*
^{34}*University of Illinois at Chicago, Chicago, Illinois 60607*
^{35}*Southern Connecticut State University, New Haven, CT, 06515*
^{36}*Purdue University, West Lafayette, Indiana 47907*
^{37}*Valparaiso University, Valparaiso, Indiana 46383*
^{38}*Warsaw University of Technology, Warsaw 00-661, Poland*
^{39}*Temple University, Philadelphia, Pennsylvania 19122*
^{40}*University of Science and Technology of China, Hefei, Anhui 230026*
^{41}*National Cheng Kung University, Tainan 70101*
^{42}*Indiana University, Bloomington, Indiana 47408*
^{43}*State University Of New York, Stony Brook, NY 11794*
^{44}*Wayne State University, Detroit, Michigan 48201*
^{45}*Frankfurt Institute for Advanced Studies FIAS, Frankfurt 60438, Germany*
^{46}*Argonne National Laboratory, Argonne, Illinois 60439*
^{47}*Indian Institute of Technology, Mumbai 400076, India*
^{48}*Michigan State University, East Lansing, Michigan 48824*
^{49}*Pusan National University, Pusan 46241, Korea*
^{50}*Institute of Nuclear Physics PAN, Cracow 31-342, Poland*
^{51}*Lehigh University, Bethlehem, PA, 18015*
^{52}*Max-Planck-Institut fur Physik, Munich 80805, Germany*
^{53}*World Laboratory for Cosmology and Particle Physics (WLCAPP), Cairo 11571, Egypt*
^{54}*United States Naval Academy, Annapolis, Maryland, 21402*

We present a measurement of the inclusive production of Υ mesons in U+U collisions at $\sqrt{s_{NN}} = 193$ GeV at mid-rapidity ($|y| < 1$). Previous studies in central Au+Au collisions at $\sqrt{s_{NN}} = 200$ GeV show a suppression of Υ(1S+2S+3S) production relative to expectations from the Υ yield in $p+p$ collisions scaled by the number of binary nucleon-nucleon collisions (N_{coll}), with an indication that the Υ(1S) state is also suppressed. The present measurement extends the number of participant nucleons in the collision (N_{part}) by 20% compared to Au+Au collisions, and allows us to study a system with higher energy density. We observe a suppression in both the Υ(1S+2S+3S) and Υ(1S) yields in central U+U data, which consolidates and extends the previously observed suppression trend in Au+Au collisions.

I. INTRODUCTION

Quarkonium production in high energy heavy-ion collisions is expected to be sensitive to the energy density and temperature of the medium created in these collisions. Dissociation of different quarkonium states due to color screening is predicted to depend on their binding energies [1–3]. Measuring the yields of different quarkonium states therefore may serve as a model-dependent measure of the temperature in the medium [4]. Although charmonium suppression was anticipated as a key signature of the formation of a quark-gluon plasma (QGP) [5], the suppression of J/ψ mesons has been found to be relatively independent of beam energy from Super Proton Synchrotron (SPS) to Relativistic Heavy Ion Collider (RHIC) energies [6]. This phenomenon can be attributed

to J/ψ regeneration by the recombination of uncorrelated c-$\bar{c}$ pairs in the deconfined medium [7] that counterbalances the dissociation process. In addition, cold nuclear matter (CNM) effects, dissociation in the hadronic phase, and feed-down contributions from excited charmonium states and B hadrons can alter the suppression pattern from what would be expected from Debye screening. Contrary to the more abundantly produced charm quarks, bottom pair recombination and co-mover absorption effects are predicted to be negligible at RHIC energies [8]. Bottomonium states in heavy-ion collisions therefore can serve as a cleaner probe of the medium, although initial state effects may still play an important role [9–13]. Feed-down from χ_b mesons, the yield of which is largely unknown at RHIC energies, may also give a non-negligible contribution to the bottomonium yields.

Monte Carlo Glauber simulations show that collisions of large, deformed uranium nuclei reach on average a higher number of participant nucleons (N_{part}) and higher number of binary nucleon-nucleon collisions (N_{coll}) than gold-gold collisions of the same centrality class. It was estimated that central U+U collisions at $\sqrt{s_{NN}}$=193 GeV have an approximately 20% higher energy density, thus higher temperature, than that in central Au+Au collisions at $\sqrt{s_{NN}}$=200 GeV [14, 15]. Lattice quantum-chromodynamics (QCD) calculations at finite temperature suggest that the color screening radius decreases with increasing temperature as $r_D(T) \sim 1/T$, which implies that a given quarkonium state cannot form above a certain temperature threshold [16]. Free-energy-based spectral function calculations predict that the excited $\Upsilon(2S+3S)$ states cannot exist above $1.2T_c$ and that the ground state $\Upsilon(1S)$ cannot exist above approximately $2T_c$, where T_c is the critical temperature of the phase transition [4]. Around the onset of deconfinement, one may see a sudden drop in the production of a given Υ state when the threshold temperature of that state (or of higher mass states that decay into it) is reached. According to Ref. [14], in the 5% most central U+U collisions at $\sqrt{s_{NN}} = 193$ GeV, T/T_c is between 2 and 2.7, depending on the Υ formation time chosen in calculations. For a given formation time, the value of T/T_c is approximately 5% higher than in the 5% most central Au+Au collisions at $\sqrt{s_{NN}} = 200$ GeV. In such a scenario the temperature present in central U+U collisions is high enough that even the $\Upsilon(1S)$ state might dissociate. However, the finite size, lifetime and inhomogeneity of the plasma may complicate this picture and smear the turn-on of the melting of particular quarkonium states over a wide range of N_{part}. The suppression of bottomonium states in U+U collisions, together with existing measurements in other collision systems as well as measurements of CNM effects, may provide the means to explore the turn-on characteristics of suppression and test the sequential melting hypothesis.

II. EXPERIMENT AND ANALYSIS

This analysis uses data recorded in 2012 by the STAR experiment at RHIC in U+U collisions at $\sqrt{s_{NN}} = 193$ GeV. We reconstruct the Υ states via their dielectron decay channels, $\Upsilon \rightarrow e^+ e^-$, based on the method decribed in Ref. [13].

As a trigger we require at least one tower from the Barrel Electromagnetic Calorimeter (BEMC) [17] within the pseudorapidity range $|\eta| < 1$, containing a signal corresponding to an energy deposit that is higher than approximately 4.2 GeV. A total of 17.2 million BEMC-triggered events are analyzed, corresponding to an integrated luminosity of 263.4 μb^{-1}. The electron (or positron) candidate that caused the trigger signal is paired with other electron candidates within the same event. Tracks are reconstructed in the Time Projection Chamber (TPC) [18]. Electrons with a momentum $p > 1.5$ GeV/c are selected based on their specific energy loss (dE/dx) in the TPC. Candidates are required to lie within an asymmetric window of $-1.2 < n\sigma_e < 3$, where $n\sigma_e$ is the deviation of the measured dE/dx with respect to the nominal dE/dx value for electrons at a given momentum, calculated using the Bichsel parametrization [19], normalized with the TPC resolution. Figure 1 shows the efficiency of the $n\sigma_e$ cut ($\varepsilon_{n\sigma_e}$) for single electrons versus transverse momentum (p_T), determined using a high purity electron sample obtained from gamma conversions. Since most of these so-called photonic electron pairs are contained in the very low invariant mass (m_{ee}) regime, we select e^+e^- pairs with $m_{ee} < 150$ MeV/c^2 ($m_{ee} < 50$ MeV/c^2 in systematics checks) in a similar manner to the analysis described in Ref. [20].

To further enhance the purity of the electron sample we use the particle discrimination power of the BEMC. Electromagnetic showers tend to be more compact than hadron showers, and deposit their energy in fewer towers. The total energy deposit of an electron candidate ($E_{cluster}$) is determined by finding a *seed* tower with a high energy deposit (E_{tower}), and forming a *cluster* by joining the two highest-energy neighbours to this seed. An $R = \sqrt{\Delta\varphi^2 + \Delta\eta^2} < 0.04$ matching cut is applied on the distance of the seed tower position in the BEMC and the TPC track projected to the BEMC plane, expressed in azimuthal angle and pseudorapidity units. We reconstruct the quantity $E_{cluster}/p$ for each electron candidate, where p is the momentum of the electron candidate measured in the TPC. Electrons travelling close to the speed of light are expected to follow an $E_{cluster}/p$ distribution centered at c, smeared by the TPC and BEMC detector resolutions. Therefore a $0.75c < E_{cluster}/p < 1.4c$ cut is applied to reject hadron background. The efficiency of this cut for single electrons ($\varepsilon_{E/p}$), obtained from detector simulation studies, is shown in Fig. 2. Since the trigger is already biased towards more compact clusters, an Υ candidate requires that the daughter electron candidate that fired the trigger fulfills a strict condition of $E_{tower}/E_{cluster} > 0.7$, while the daughter paired to it is required to fulfill a looser $E_{tower}/E_{cluster} > 0.5$ cut.

The acceptance, as well as the tracking, the triggering and the BEMC cut efficiency correction factors are determined using simulations, where the $\Upsilon(nS) \rightarrow e^+e^-$ processes (n=1,2,3) are embedded into U+U collision events, and then reconstructed in the same way as real data. The efficiency of the dE/dx cut is determined by using the single electron efficiency from photonic electrons, as shown in Fig. 1. The BEMC-related reconstruction efficiencies are also verified with a sample of electrons identified in the TPC. Figure 3 shows the reconstruction efficiencies for $\Upsilon(1S)$, $\Upsilon(2S)$
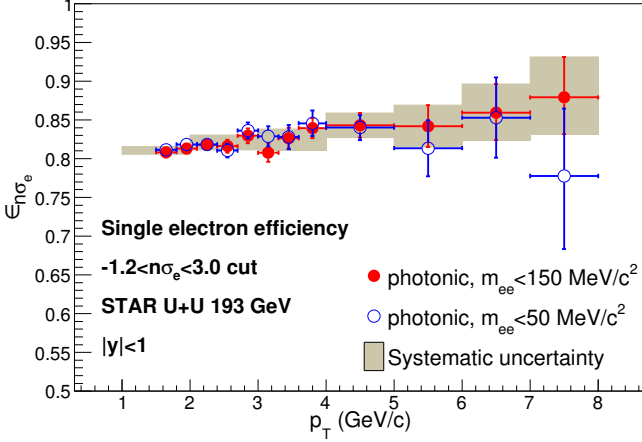
FIG. 1. *(Color online)* Single electron efficiency of the dE/dx cut versus transverse momentum, as determined by fits to $n\sigma_e$ distributions of photonic electrons. The fit errors using the sample with the $m_{ee} < 150$ MeV/c^2 photonic electron cut in 1 GeV/c wide bins are used as systematic uncertainties. The results using the $m_{ee} < 50$ MeV/c^2 photonic electron cut are consistent with the former one.
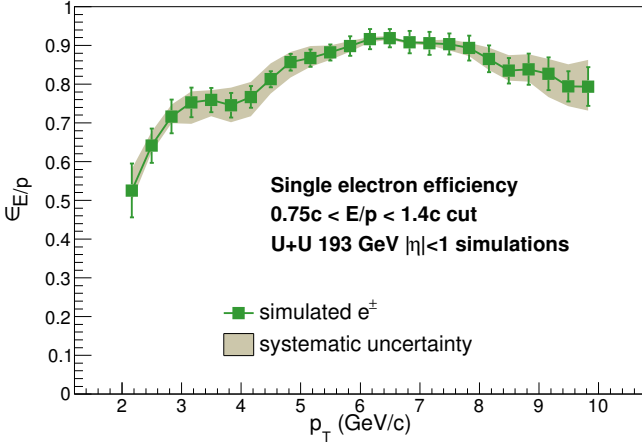

FIG. 2. *(Color online)* Single electron efficiency of the E_{cluster}/p cut versus transverse momentum. The efficiency corrections are obtained from embedded simulations. The difference between the default result from simulations and that extracted using a pure electron sample from data is taken as the systematic uncertainty.

FIG. 3. *(Color online)* Reconstruction efficiencies for $\Upsilon(1S)$, $\Upsilon(2S)$ and $\Upsilon(3S)$, as determined from embedded simulations and identified electron samples. Cuts for *i)* acceptance, triggering and tracking, *ii)* specific energy loss, *iii)* track–cluster matching, *iv)* E_{cluster}/p and *v)* cluster compactness ($E_{\text{tower}}/E_{\text{cluster}}$) are applied consecutively to build up the total reconstruction efficiency. The efficiencies corresponding to each cut are shown stacked in a top-to-bottom order. Black ticks at the end of each bar represent the total uncertainties on the given efficiency. The p_T-binned values correspond to 0-60% centrality.

and $\Upsilon(3S)$ states separately, for 0–60% centrality, as well as for centrality bins 0–10%, 10–30%, 30–60%, and transverse momentum bins of $p_T < 2$ GeV/c, $2 < p_T < 4$ GeV/c and $4 < p_T < 10$ GeV/c.

The invariant mass spectrum of the Υ candidates is reconstructed within the rapidity window $|y| < 1$ using dielectron momenta measured in the TPC. Figure 4 shows the m_{ee} distribution of unlike-sign pairs as solid circles, along with the sum of the positive and negative like-sign distributions as open circles. The data are divided into three centrality bins, shown in Fig. 5, and three p_T bins. The measured signal from each
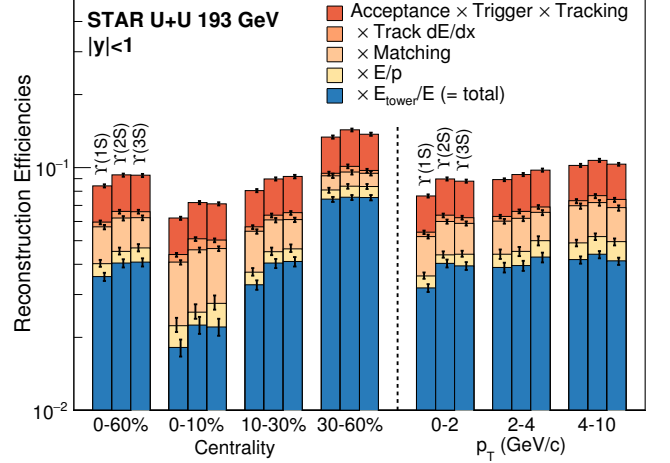
of the $\Upsilon(nS) \to e^+e^-$ processes ($n = 1,2,3$) is parametrized with a Crystal Ball function [21], with parameters obtained from fits to the $\Upsilon(nS)$ mass peaks from simulations. Such a shape was justified by preceding studies [22] and accounts for the effects of Bremsstrahlung and the momentum resolution of the TPC. The combinatorial background is modelled with a double exponential function. In addition, there is a sizeable correlated background from $b\bar{b}$ decays and Drell-Yan processes. Based on previous studies [13, 22] we use a ratio of two power law functions that were found to adequately describe these contributions. In order to determine the Υ yield, a simultaneous log-likelihood fit is performed on the like-sign and the unlike-sign data. The unlike-sign data are fitted with a function that includes the combinatorial and correlated background shapes plus the three Υ mass peaks, while the like-sign data is fitted with the combinatorial background shape only. The parameters of the mass peaks and those of the correlated background are fixed in the fit according to the simulations and previous studies [13, 22], respectively, except for normalization parameters. The contribution of each $\Upsilon(nS)$ state to the total $\Upsilon(1S+2S+3S)$ yield is determined based on the integral of the individual Crystal Ball functions that are fit to the measured peaks. The uncertainties quoted as statistical are the uncertainties from the fit.
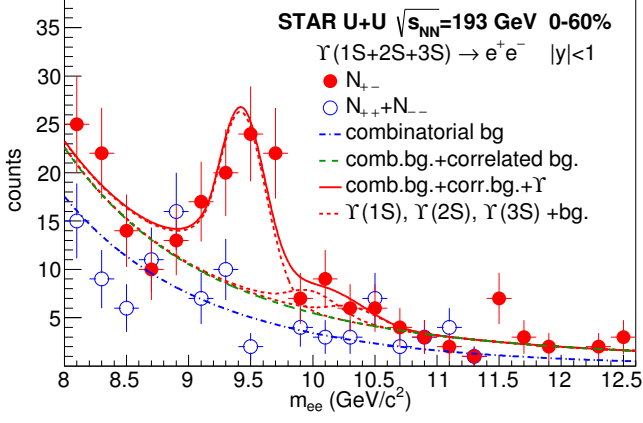
FIG. 4. *(Color online)* Reconstructed invariant mass distribution of Υ candidates (unlike-sign pairs, denoted as solid circles) and like-sign combinatorial background (open circles) in U+U collisions at $\sqrt{s_{NN}} = 193$ GeV for 0-60% centrality at mid-rapidity ($|y| < 1$). Fits to the combinatorial background, $b\bar{b}$ and Drell-Yan contributions and to the Υ peaks are plotted as dash-dotted, dashed and solid lines respectively. The fitted contributions of the individual $\Upsilon(1S)$, $\Upsilon(2S)$ and $\Upsilon(3S)$ states are shown as dotted lines.

III. SYSTEMATIC UNCERTAINTIES

We consider several sources of systematic uncertainties in the present study. Geometrical acceptance is affected by Υ polarization as well as by noisy towers that are not used in the reconstruction. The sytematics stemming from these factors, estimated in Ref. [13], are taken as fully correlated between collision systems. The geometrical acceptance correction factor is dependent on the p_T and rapidity distributions of the Υ mesons. We assume a Boltzmann-like p_T-distribution, $\frac{dN}{dp_T} \propto \frac{p_T}{\exp(p_T/p_0)+1}$, in our embedded simulations. We obtain its slope parameter of $p_0 = 1.11$ GeV/c from a parametrized interpolation of $p+p$ data from ISR, CDF and measurements [23–25], similar to Ref. [13]. Although this value matches the fit to the p_T spectrum of the current analysis, detailed in Sec. IV, there is a slight difference between the two within the statistical error range. The uncertainty from the slope is determined by adjusting the slope to match the fitted value, $p_0 = 1.37$ GeV/c. The rapidity distribution is determined using PYTHIA [26] version 8.1 to follow an approximately Gaussian shape with $\sigma = 1.15$. We vary the width between 1.0 and 1.16 to cover the range of the uncertainties of the Gaussian fit, as well as estimations of earlier studies [13].

The uncertainty of the TPC track reconstruction efficiency caused by the variation in operational conditions was studied in Refs. [13, 27]. The errors of the Gaussian fits to the $n\sigma_e$ distribution of photonic electrons are taken as the uncertainties on the electron identification using TPC (dE/dx). Changing the photonic electron selection from the default $m_{ee} < 150$ MeV/c^2 to $m_{ee} < 50$ MeV/c^2, or using TPC-identified electrons instead of photonic ones yield a result that is consistent with the default choice within systematic uncertainties. Fig-
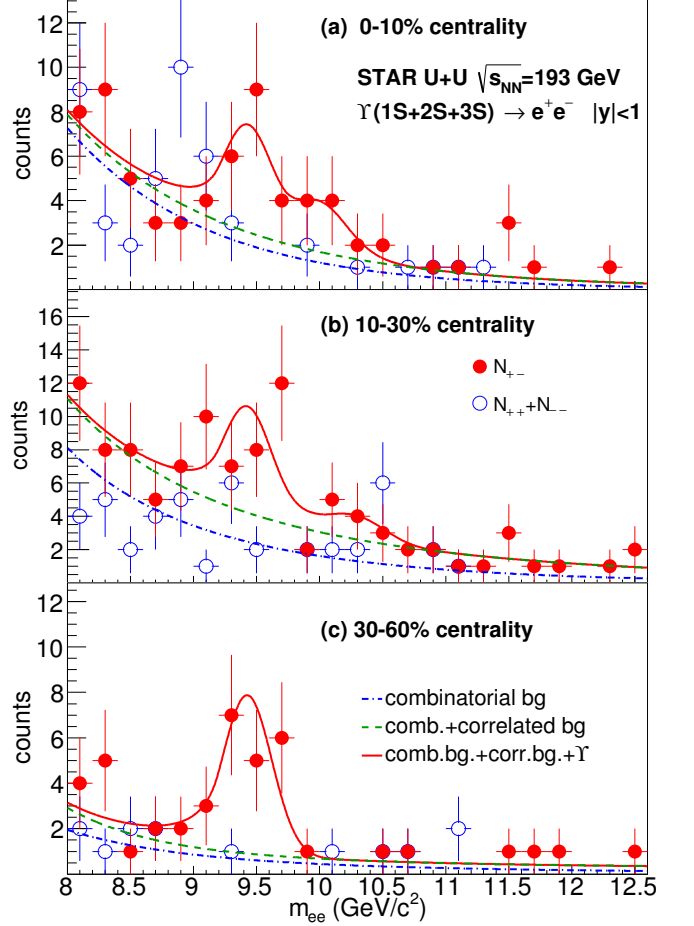

FIG. 5. *(Color online)* Reconstructed invariant mass distribution of Υ candidates (solid circles) and like-sign combinatorial background (open circles) in U+U collisions at $\sqrt{s_{NN}} = 193$ GeV for p_T-integrated 0-10% (a) 10-30% (b) 30-60% (c) centralities at mid-rapidity ($|y| < 1$). Fits to the combinatorial background, $b\bar{b}$ and Drell-Yan contributions and the peak fits are plotted as dash-dotted, dashed and solid lines respectively.

ure 1 shows the systematic uncertainty corresponding to the dE/dx single electron efficiency as a band around the data points. The uncertainty stemming from the trigger turn-on characteristics, from the criteria of electron selection with the BEMC (matching, $E_{cluster}/p$, as well as the cluster compactness $E_{tower}/E_{cluster}$) are determined from the comparison of efficiencies calculated from embedded simulations and from electron samples obtained from data using TPC (dE/dx) identification and reconstructed photonic conversion electrons. The dominant source of systematic uncertainty among those listed above is the uncertainty of the $E_{cluster}/p$ cut efficiency. In Fig. 2 we indicate the systematic uncertainty corresponding to the single electron $E_{cluster}/p$ efficiency with a band around the data points.

Another major source of uncertainty arises from the assumptions of the signal and background shapes made in extracting the signal yield. The extraction method was system-

centrality	N_{part}	N_{coll}
0-60%	188.3±5.5	459±10
0-10%	385.1±9	1146±49
10-30%	236.2±14	574±41
30-60%	91.0±32	154±37

TABLE I. The N_{coll} and N_{part} values corresponding to different centrality ranges, obtained using the Monte Carlo Glauber model.

Source of systematic uncertainty	value (%)
Number of binary collisions (R_{AA}-only)	2.2
Geometrical acceptance (yield-only)	$+1.7$ -3.0
p_{T} and y distributions	2.1
Trigger efficiency	$+1.1$ -3.6
Tracking efficiency	11.8
TPC dE/dx	$+4.0$ -6.4
TPC–BEMC matching	5.4
BEMC E_{cluster}/p	$+8.8$ -13.2
BEMC $E_{\text{tower}}/E_{\text{cluster}}$	2.0
Signal extraction — $\Upsilon(1S+2S+3S)$	$+8.4$ -7.0
Signal extraction — $\Upsilon(1S)$	$+11.9$ -5.7
Signal extraction — $\Upsilon(2S+3S)$	$+5.3$ -19.7

TABLE II. Major systematic uncertainties excluding common normalization uncertainties from the $p+p$ reference, for 0-60% centrality data.

states	centrality	$B_{ee} \times (d\sigma_{AA}^{\Upsilon}/dy)$ (μb)	R_{AA}^{Υ}
$\Upsilon(1S+2S+3S)$	0–60%	$4.27 \pm 0.90^{+0.90}_{-0.82}$	$0.82 \pm 0.17^{+0.14}_{-0.11}$
	0–10%	$6.64 \pm 4.22^{+1.95}_{-1.66}$	$0.51 \pm 0.32^{+0.13}_{-0.11}$
	10–30%	$3.67 \pm 1.62^{+1.04}_{-0.78}$	$0.56 \pm 0.25^{+0.14}_{-0.10}$
	30–60%	$3.42 \pm 1.04^{+0.57}_{-0.97}$	$1.96 \pm 0.59^{+0.51}_{-0.68}$
$\Upsilon(1S)$	0–60%	$3.55 \pm 0.77^{+0.80}_{-0.66}$	$0.96 \pm 0.21^{+0.18}_{-0.13}$
	0–10%	$4.52 \pm 2.08^{+1.31}_{-1.13}$	$0.49 \pm 0.23^{+0.12}_{-0.10}$
	10–30%	$2.91 \pm 1.10^{+0.85}_{-0.61}$	$0.63 \pm 0.24^{+0.17}_{-0.11}$
	30–60%	$3.42 \pm 0.95^{+0.57}_{-0.97}$	$2.76 \pm 0.76^{+0.71}_{-0.95}$
$\Upsilon(2S+3S)$	0–60%	$0.72 \pm 0.49^{+0.15}_{-0.19}$	$0.48 \pm 0.32^{+0.07}_{-0.11}$
	0–10%	$2.11 \pm 3.33^{+0.64}_{-0.54}$	$0.56 \pm 0.89^{+0.15}_{-0.12}$
	10–30%	$0.76 \pm 1.03^{+0.29}_{-0.16}$	$0.41 \pm 0.55^{+0.15}_{-0.07}$

TABLE III. Cross-sections multiplied by the branching ratio of the leptonic channel, and nuclear modification of $\Upsilon(1S+2S+3S)$ mesons, the ground states and the excited states separately, in 0–60% U+U collisions as well as in each centrality bin. The uncertainties are listed statistical first and systematic second. The statistical uncertainties from the $p+p$ reference, not included in the table, are 12.7%, 13.0% and 30% for the $\Upsilon(1S+2S+3S)$, $\Upsilon(1S)$ and $\Upsilon(2S+3S)$ respectively. There is an additional 11% common normalization uncertainty on R_{AA} from the $p+p$ luminosity estimation [13].

atically modified to estimate the uncertainties from momentum resolution and calibration, functional shapes of the correlated and combinatorial backgrounds as well as the signal, and those from the fit range in the following ways: *i)* An additional 50 MeV/c^2 smearing was added to the peaks to model a worst-case scenario in the momentum resolution [22]; *ii)* The double exponential fit function used for the combinatorial background was replaced with a single exponential function; *iii)* Instead of modelling the correlated background with a ratio of two power law functions, we used a single power law function to commonly represent the Drell-Yan and $b\bar{b}$ contributions, and we also tested the sum of these two functions to represent the Drell-Yan and $b\bar{b}$ contributions individually in the fitting; *iv)* Finally, we moved the lower and upper limits of the simultaneous fit range in several steps from 6.6 to 8.0 GeV/c^2 and from 15.4 to 12.4 GeV/c^2 respectively. The Υ yields were determined in each case, and the maximum deviation from the default case in positive or negative direction was taken as the signal extraction uncertainty.

We construct the nuclear modification factor, R_{AA}, to quantify the medium effects on the production of the Υ states. The R_{AA} is computed by comparing the corrected number of Υ mesons measured in A+A collisions to the yield in $p+p$ collisions scaled by the average number of binary nucleon-nucleon collisions, as $R_{\text{AA}}^{\Upsilon} = \frac{\sigma_{pp}^{inel}}{\sigma_{AA}^{inel}} \frac{1}{\langle N_{\text{coll}} \rangle} \frac{B_{ee} \times (d\sigma_{\Upsilon}^{AA}/dy)}{B_{ee} \times (d\sigma_{\Upsilon}^{pp}/dy)}$, where $\sigma_{AA(pp)}^{inel}$ is the total inelastic cross-section of the U+U ($p+p$) collisions, $d\sigma_{\Upsilon}^{AA(pp)}/dy$ denotes the Υ production cross-section in U+U ($p+p$) collisions, and B_{ee} is the branching ratio of the $\Upsilon \to e^+e^-$ process. Our reference was measured in $p+p$ collisions at $\sqrt{s} = 200$ GeV [22], and has to be scaled to $\sqrt{s} = 193$ GeV. Calculations for the $p+p$ inelastic cross-section [28] yield a 0.5% smaller value at $\sqrt{s} = 193$ GeV than at $\sqrt{s} = 200$ GeV. The Υ production cross-section, however, shows a stronger dependence on the collision energy. Both the NLO color-evaporation model calculations, which describe the world $p+p$ data [29], and a linear interpolation of the same data points within the RHIC-LHC energy regime yield an approximately 4.6% decrease in the cross section when $\sqrt{s}$ is changed from 200 to 193 GeV. The uncertainties do not exceed 0.5% (absolute) in any of these corrections, and are thus neglected. The values used to compute R_{AA} are $B_{ee} \times (d\sigma_{\Upsilon}^{pp}/dy)\big|_{|y|<1} = 60.64$ pb, $\sigma_{pp}^{inel} = 42.5$ mb and $\sigma_{UU}^{inel} = 8.14$ b. The N_{part} and N_{coll} values used in this analysis, computed using the Monte Carlo Glauber model [30] following the method of Ref. [31], are listed in Table I.

The systematic uncertainties for U+U collisions at 0-60%

centrality are summarized in Table II. The total relative systematic uncertainty on R_{AA}^{Υ}, calculated as a quadratic sum of the uncertainties listed in the table excluding common normalization uncertainties from the $p+p$ reference measurements, ranges from 15% to 27% dependent on centrality and p_{T}.

IV. RESULTS

The production cross-sections are summarized in Table III for the sum of all three Υ states, the separated $\Upsilon(1S)$ state, and for the excited $\Upsilon(2S+3S)$ states together. Table IV lists the cross-sections in the given p_{T} ranges for $\Upsilon(1S+2S+3S)$ and

states	p_T (GeV/c)	$B_{ee} \times \frac{d^2\sigma^\Upsilon_{AA}}{dp_T dy}\left(\frac{\mu b}{GeV/c}\right)$
Υ(1S+2S+3S)	0–2	$1.40 \pm 0.49^{+0.36}_{-0.23}$
	2–4	$1.96 \pm 0.51^{+0.42}_{-0.43}$
	4–10	$0.53 \pm 0.77^{+0.20}_{-0.11}$
Υ(1S)	0–2	$1.30 \pm 0.39^{+0.28}_{-0.22}$
	2–4	$1.61 \pm 0.43^{+0.35}_{-0.35}$
	4–10	$0.30 \pm 0.38^{+0.17}_{-0.05}$

TABLE IV. Cross-sections multiplied by the branching ratio of the leptonic channel, in given p_T ranges for the Υ(1S+2S+3S) and Υ(1S) states in 0–60% U+U collisions.

Υ(1S). The p_T spectrum is well described by a Boltzmann distribution with a slope parameter of $p_0^{\Upsilon(1S+2S+3S)} = (1.37 \pm 0.20^{+0.03}_{-0.07})$ GeV/c and $p_0^{\Upsilon(1S)} = (1.22 \pm 0.15 \pm^{+0.04}_{-0.05})$ GeV/c. These values are consistent with the interpolation from $p+p$ data within uncertainties.

The Υ(1S+2S+3S) and Υ(1S) nuclear modification factors as a function of N_{part} are shown in Fig. 6, and compared to the nuclear modification factor in Au+Au data at $\sqrt{s_{NN}} = 200$ GeV from STAR [13] at $|\eta| < 1$, PHENIX [32] at $|\eta| < 0.35$, and in Pb+Pb data measured by CMS at $\sqrt{s_{NN}} = 2.76$ TeV via the $\Upsilon \to \mu^+\mu^-$ channel within $|\eta| < 2.4$ [33]. The data points in the 30-60% centrality bin have large statistical and systematical uncertainties, providing little constraint on R_{AA}. In Figs. 6 and 7 we therefore only show the 95% lower confidence bound for these points, derived by quadratically adding statistical and point-to-point systematic uncertainties. The R_{AA} values measured in all N_{part} bins for the Υ(1S+2S+3S), Υ(1S) and Υ(2S+3S) states are summarized in Table III. Note that the Υ(1S) results are not corrected for feed-down from the excited states.

The trend marked by the Au+Au $R_{AA}(N_{part})$ points is augmented by the U+U data. We observe neither a significant difference between the results in any of the centrality classes, nor do we find any evidence of a sudden increase in suppression in central U+U compared to the central Au+Au data, although the precision of the current measurement does not exclude a moderate drop in R_{AA}. Assuming that the difference in suppression between the Au+Au and U+U collisions is small, the two data sets can be combined. We carry out the unification using the BLUE method [34, 35] with the conservative assumption that all common systematic uncertainties are fully correlated. We find that Υ(1S) production is significantly suppressed in central heavy-ion collisions at top RHIC energies, but this suppression is not complete: $R_{AA}^{\Upsilon(1S)} = 0.63 \pm 0.16 \pm 0.09$ where the first uncertainty includes both the unified statistical and systematic errors and the second one is the global scaling uncertainty from the $p+p$ reference. While both the RHIC and LHC data show suppression in the most central bins, $R_{AA}^{\Upsilon(1S)}$ is slightly, although not significantly, higher in RHIC semi-central collisions than in the LHC. In the Au+Au data, the Υ(2S+3S) excited states have been found to be strongly suppressed, and an upper limit $R_{AA}^{\Upsilon(2S+3S)} < 0.32$ was established. The Υ(2S+3S) suppression
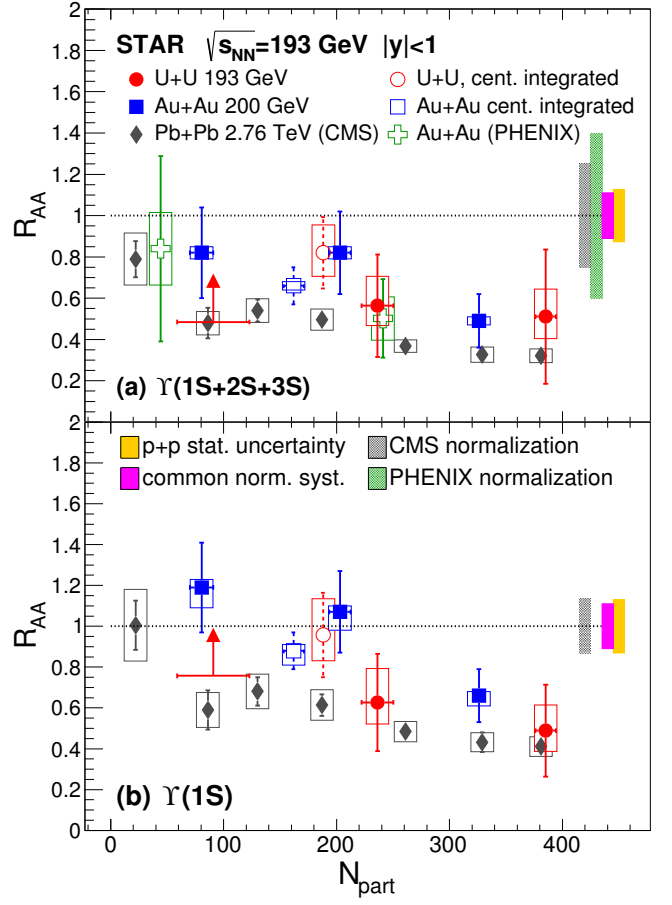

FIG. 6. *(Color online)* Υ(1S+2S+3S) (a) and Υ(1S) (b) R_{AA} vs. N_{part} in $\sqrt{s_{NN}} = 193$ GeV U+U collisions (solid circles), compared to 200 GeV RHIC Au+Au (solid squares [13] and hollow crosses [32]), and 2.76 TeV LHC Pb+Pb data (solid diamonds [33]). A 95% lower confidence bound is indicated for the 30-60% centrality U+U data (see text). Each point is plotted at the center of its bin. Centrality integrated (0-60%) U+U and Au+Au data are also shown as open circles and squares, respectively.

observed in U+U data is consistent with this upper limit.

In Fig. 7 we compare STAR measurements to different theoretical models [36–38]. An important source of uncertainty in model calculations for quarkonium dissociation stems from the unknown nature of the in-medium potential between the quark-antiquark pairs. Two limiting cases that are often used are the internal-energy-based heavy quark potential corresponding to a strongly bound scenario (SBS), and the free-energy-based potential corresponding to a more weakly bound scenario (WBS) [9]. The model of Emerick, Zhao and Rapp [36] includes CNM effects, dissociation of bottomonia in the hot medium (assuming a temperature $T = 330$ MeV) and regeneration for both the SBS and WBS scenarios. The Strickland-Bazow model [37] calculates dissociation in the medium in both a free-energy-based "model A" and an internal-energy-based "model B", with an initial central temperature $428 < T < 442$ MeV. The model of Liu *et al.* [38] uses an internal-energy-based potential and an in-
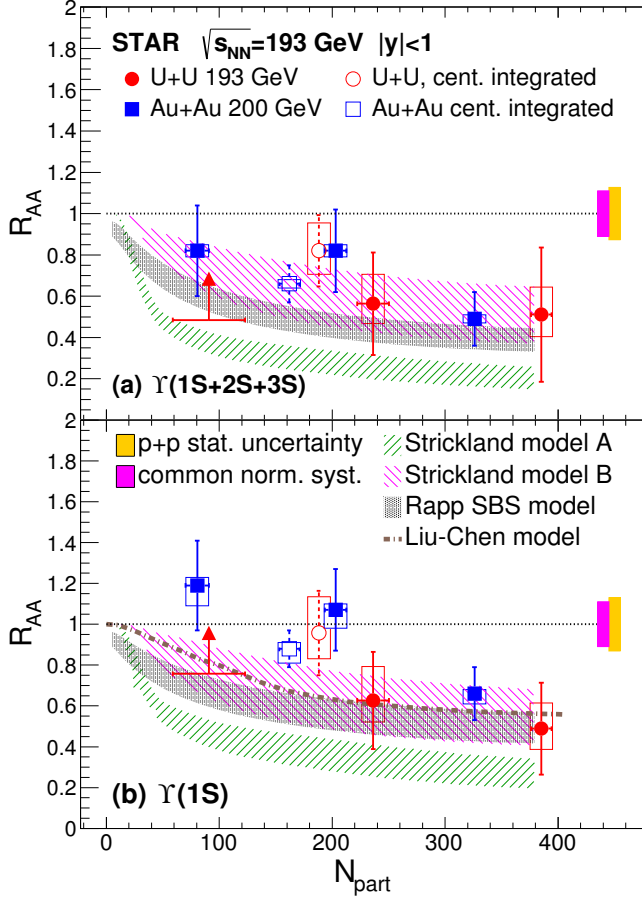
FIG. 7. *(Color online)* Υ(1S+2S+3S) (a) and Υ(1S) (b) R_{AA} vs. N_{part} in $\sqrt{s_{NN}}$ = 193 GeV U+U collisions (solid circles), compared to different models [36–38], described in the text. The 95% lower confidence bound is indicated for the 30-60% centrality U+U data (see text). Each point is plotted at the center of its bin. Centrality integrated (0-60%) U+U and Au+Au data are also shown as open circles and squares, respectively.

FIG. 8. *(Color online)* Quarkonium R_{AA} versus binding energy in Au+Au and U+U collisions. Open symbols represent 0-60% centrality data, filled symbols are for 0-10% centrality. The Υ measurements in U+U collisions are denoted by red points. In the case of Au+Au collisions, the Υ(1S) measurement is denoted by a blue square, while for the Υ(2S+3S) states, a blue horizontal line indicates a 95% upper confidence bound. The black diamonds mark the high-p_T J/ψ measurement. The vertical lines represent nominal binding energies for the Υ(1S) and J/ψ, calculated based on the mass defect, as $2m_D - m_{J/\psi}$ and $2m_B - m_\Upsilon$, respectively (where m_X is the mass of the given meson X) [39]. The shaded area spans between the binding energies of Υ(2S) and Υ(3S). The data points are slightly shifted to the left and right from the nominal binding energy values to improve their visibility.

put temperature $T = 340$ MeV. In Fig. 7 we show all three internal-energy-based models together with the "model A" of Ref. [37] as an example for the free-energy-based models. The internal-energy-based models generally describe RHIC data well within the current uncertainties, while the free-energy-based models tend to underpredict the R_{AA} especially for the Υ(1S).

Figure 8 shows the R_{AA} versus binding energy of Υ(1S) and Υ(2S+3S) states [39] in U+U and Au+Au collisions. The results are also compared to high-p_T J/ψ in Au+Au collisions [40]. This comparison is motivated by the expectation from model calculations, e.g. that in Ref. [41], that charm recombination is moderate at higher momenta. Recent measurements at the LHC [42, 43] indicate that the suppression of the Υ production, as well as that of the prompt J/ψ in the $p_T > 5$ GeV/c range, is rather independent of the momentum of the particle. Contrary to earlier assumptions [44, 45], no noticeable p_T or rapidity dependence was observed. However, the non-prompt J/ψ production [43], originating dominantly
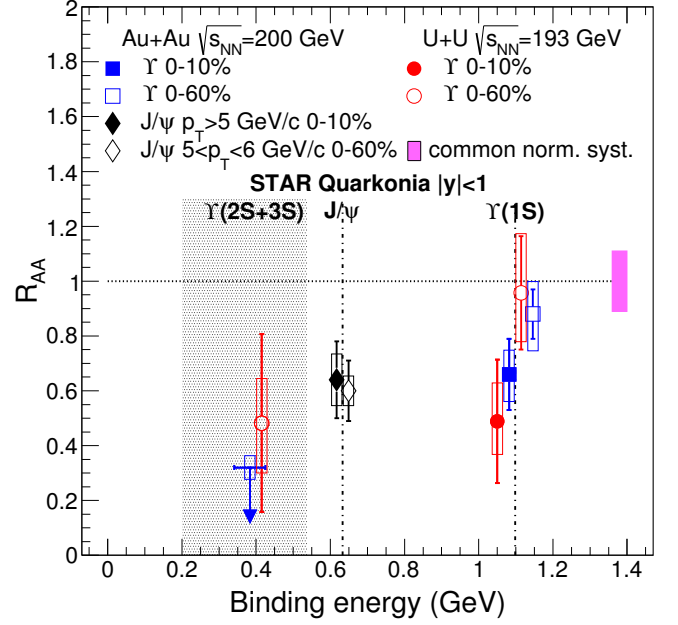
from B meson decays, does show a clear p_T dependence [40]. This affects the pt-dependence of inclusive J/ψ production, especially at high-p_T. Our current data does not have sufficient statistics to study the p_T dependence of the Υ in detail and to verify whether the observations at the LHC also hold at RHIC energies. The results in U+U collisions are consistent with the Au+Au measurements as well as with the expectations from the sequential melting hypothesis.

V. SUMMARY

We presented mid-rapidity measurements of inclusive bottomonium production in U+U collisions at $\sqrt{s_{NN}}$ = 193 GeV. The cross-section is $B_{ee} \times (d\sigma_{AA}^\Upsilon/dy) = 4.27 \pm 0.90^{+0.90}_{-0.82}$ μb for the Υ(1S+2S+3S), and $B_{ee} \times (d\sigma_{AA}^{\Upsilon(1S)}/dy) = 3.55 \pm 0.77^{+0.80}_{-0.66}$ μb for the separated Υ(1S) state.

The present measurements increased the range of the number of participants in the collision compared to the previous Au+Au measurements by approximately 20%. A signifi-

cant suppression is observed in central U+U data for both the $\Upsilon(1S+2S+3S)$ ($R_{AA}^{\Upsilon} = 0.51 \pm 0.32^{+0.13}_{-0.11} \pm 0.08$, where the first uncertainty reflects the statistical error, the second the overal systematic uncertainty, and the third the uncertainty from the $p+p$ reference) and $\Upsilon(1S)$ ($R_{AA}^{\Upsilon(1S)} = 0.49 \pm 0.23^{+0.12}_{-0.10} \pm 0.09$), which consolidates and extends the previously observed $R_{AA}(N_{part})$ trend in Au+Au collisions. The data from 0-60% central U+U collisions is consistent with a strong suppression of the $\Upsilon(2S+3S)$ states, which has also been observed in Au+Au collisions. Comparison of the suppression patterns from Au+Au and U+U data to different models favors an internal-energy-based quark potential scenario.

[1] S. Digal, P. Petreczky and H. Satz, Phys. Lett. B **514**, 57 (2001).
[2] C. Y. Wong, Phys. Rev. C **72**, 034906 (2005).
[3] D. Cabrera and R. Rapp, Eur. Phys. J. A **31**, 858 (2007).
[4] Á. Mócsy and P. Petreczky, Phys. Rev. Lett. **99**, 211602 (2007).
[5] T. Matsui and H. Satz, Phys. Lett. B **178**, 416 (1986).
[6] A. Adare *et al.* [PHENIX Collaboration], Phys. Rev. Lett. **98**, 232301 (2007).
[7] L. Grandchamp, R. Rapp and G. E. Brown, J. Phys. G **30**, S1355 (2004).
[8] R. Rapp, D. Blaschke and P. Crochet, Prog. Part. Nucl. Phys. **65**, 209 (2010).
[9] L. Grandchamp, S. Lumpkins, D. Sun, H. van Hees and R. Rapp, Phys. Rev. C **73**, 064906 (2006).
[10] R. Vogt, R. E. Nelson and A. D. Frawley, PoS ConfinementX, **203** (2012).
[11] F. Arleo and S. Peigne, JHEP **1303**, 122 (2013).
[12] A. Frawley [PHENIX Collaboration], Nucl. Phys. A **932**, 105 (2014).
[13] L. Adamczyk *et al.* [STAR Collaboration], Phys. Lett. B **735**, 127 (2014); L. Adamczyk *et al.* [STAR Collaboration], Phys. Lett. B **743**, 537 (2015).
[14] D. Kikola, G. Odyniec and R. Vogt, Phys. Rev. C **84**, 054907 (2011).
[15] J. T. Mitchell [PHENIX Collaboration], PoS CPOD **2013**, 003 (2013), and the corresponding talk at *Quark Matter, Int. Conf. Ultra-Rel. Nucl.-Nucl. Coll. 2012*.
[16] K. Petrov [RBC-Bielefeld Collaboration], J. Phys. G **34**, S639 (2007).
[17] M. Beddo *et al.* [STAR Collaboration], Nucl. Instrum. Meth. A **499**, 725 (2003).
[18] K. H. Ackermann *et al.* [STAR Collaboration], Nucl. Instrum. Meth. A **499**, 624 (2003).
[19] H. Bichsel, Nucl. Instrum. Meth. A **562**, 154 (2006).
[20] H. Agakishiev *et al.* [STAR Collaboration], Phys. Rev. D **83**, 052006 (2011).
[21] J. Gaiser, SLAC Stanford - SLAC-255 (82,REC.JUN.83) 194p.
[22] B. I. Abelev *et al.* [STAR Collaboration], Phys. Rev. D **82**, 012004 (2010).
[23] D. Acosta *et al.* [CDF Collaboration], Phys. Rev. Lett. **88**, 161802 (2002).
[24] C. Kourkoumelis *et al.*, Phys. Lett. B **91**, 481 (1980).
[25] V. Khachatryan *et al.* [CMS Collaboration], Phys. Rev. D **83**, 112004 (2011).
[26] T. Sjöstrand, Comput. Phys. Commun. **82**, 74 (1994).
[27] C. Adler *et al.* [STAR Collaboration], Phys. Rev. Lett. **87**, 112303 (2001).
[28] G. A. Schuler and T. Sjöstrand, Phys. Rev. D **49**, 2257 (1994).
[29] M. Bedjidian *et al.*, hep-ph/0311048.
[30] B. Alver, M. Baker, C. Loizides and P. Steinberg, arXiv:0805.4411 [nucl-ex].
[31] H. Masui, B. Mohanty and N. Xu, Phys. Lett. B **679**, 440 (2009).
[32] A. Adare *et al.* [PHENIX Collaboration], Phys. Rev. C **91**, 024913 (2015).
[33] S. Chatrchyan *et al.* [CMS Collaboration], Phys. Rev. Lett. **109**, 222301 (2012).
[34] A. Valassi, Nucl. Instrum. Meth. A **500**, 391 (2003).
[35] R. Nisius, Eur. Phys. J. C **74**, 3004 (2014).
[36] A. Emerick, X. Zhao and R. Rapp, Eur. Phys. J. A **48**, 72 (2012).
[37] M. Strickland and D. Bazow, Nucl. Phys. A **879**, 25 (2012).
[38] Y. Liu, B. Chen, N. Xu and P. Zhuang, Phys. Lett. B **697**, 32 (2011).
[39] H. Satz, Nucl. Phys. A **783**, 249 (2007).
[40] L. Adamczyk *et al.* [STAR Collaboration], Phys. Lett. B **722**, 55 (2013).
[41] Y. Liu, Z. Qu, N. Xu and P. Zhuang, Phys. Lett. B **678**, 72 (2009).
[42] V. Khachatryan *et al.* [CMS Collaboration], arXiv:1611.01510 [nucl-ex].
[43] V. Khachatryan *et al.* [CMS Collaboration], arXiv:1610.00613 [nucl-ex].
[44] X. M. Xu, D. Kharzeev, H. Satz and X. N. Wang, Phys. Rev. C **53**, 3051 (1996).
[45] Y. Liu, N. Xu and P. Zhuang, Phys. Lett. B **724**, 73 (2013).